

**Alpha-Particles as Probes of Nuclear Shape and Structure Effects  
in Proton Evaporation Spectra**

D.G. Sarantites, N.G. Nicolis, V. Abenante, Z. Majka, T.M. Semkow

Washington University, St. Louis, MO 63130

and

C. Baktash, J.R. Beene, G. Garcia-Bermudez, M.L. Halbert, D.C. Hensley,

N.R. Johnson, I.Y. Lee, F.K. McGowan, M.A. Riley, A. Virtanen

Oak Ridge National Laboratory, Oak Ridge, TN 37830

and

H.C. Griffin

University of Michigan, Ann Arbor, MI 48109

**ABSTRACT:** The emission barriers and subbarrier anisotropies in the alpha-particle decay with respect to the spin direction of Sn and rare earth compound nuclei are examined in the light of recent calculations incorporating deformation effects in the decay process. For the Sn systems the spectral shapes and anisotropies can be explained without involving deformation. For the rare earth systems deformation which increases with spin is necessary to explain the data. Energy spectra and angular correlations of evaporated protons from the  $^{52}\text{Cr}(^{34}\text{S}, 2p2n)^{82}\text{Sr}$  reaction were measured in coincidence with discrete transitions. Large shifts in proton spectra were observed when high spin states in different rotational bands are populated. These effects cannot be explained by statistical model calculations that do not include explicitly nuclear structure effects in the deexcitation process. They are interpreted as due to near-yrast stretched proton emission, which preferentially populates the yrast band by subbarrier protons.

**1. Introduction.**

The study of nuclear shapes at high angular momentum and excitation energy is a topic of current theoretical and experimental interest in heavy-ion physics. It is well known that collective nuclei near the yrast line are deformed and their structure is well described by liquid-drop-Strutinsky cranked shell model calculations. A question of interest is the evolution of these shapes as the spin and the excitation energy (temperature) are increased. There is already considerable experimental evidence for the existence of superdeformed

nuclei ( $\beta = 0.6$ ) at high spins.<sup>1</sup> Theoretical calculations that explain these highly deformed shapes predict even higher deformations ("hyperdeformed" structures with  $\beta \approx 0.9$ ) for nuclei close to the fission stability limit<sup>2,3</sup>. Temperature-induced noncollective rotation in nuclei, as well as shape changes have also been discussed in connection with predictions of mean field theories.<sup>4</sup> A number of experimental studies have tried to explore the effect of high excitation and/or angular momentum degrees of freedom on the nuclear shapes. This is made, on one hand, by exploiting the  $\gamma$ -decay properties (for example, study of giant resonances built on excited states) of the deexciting compound nuclei<sup>5</sup>. On the other hand, extensive searches are being made to find signatures of shape effects in the charged-particle decay properties of such systems<sup>6-12</sup>.

The motivation for light charged particle studies lies in the well established fact that (fission-stable) compound nuclei, with the highest possible angular momentum, often decay by emitting alpha particles and protons. If the deexciting nucleus is deformed, it exhibits a lower evaporation barrier along the longer axis for charged-particle emission, compared to the spherical case. This results in strong enhancements of  $\alpha$  and proton decay along the long axis, especially in the energy region below the evaporation Coulomb barrier<sup>6,7,12</sup>. Simulation studies along these lines have motivated a number of experiments consisting of the observation of  $\alpha$ -particle spectra in heavy-ion fusion-evaporation reactions in a singles mode or in coincidence with evaporation residues<sup>7,11,12</sup>. The inability to reproduce the subbarrier part of the observed  $\alpha$ -spectra, with statistical model calculations assuming spherical emission shapes, has been used as an indication of a deformation effect.

The desire for enhancing the observed anisotropies for  $\alpha$ -particle emission in order to study these effects led to development of the spin alignment method with the Spin Spectrometer<sup>13</sup>, a highly segmented  $4\pi$   $\gamma$ -ray detector system. In this method, the magnitude and orientation of the spin of the residual nuclei is deduced on an event-by-event basis. This makes possible detailed studies, such as the measurement of  $\alpha$ -particle angular distributions with respect to the estimated spin direction<sup>14</sup>. Furthermore, the  $\gamma$ -multiplicity selection with the spin spectrometer allows us to study these decay characteristics as a function of the evaporation residue spin, which is closely correlated to the compound nucleus spin. Therefore, the alpha-decay properties of different compound nuclear systems can be studied in detail<sup>8-10</sup>.

In the first part of this paper, we report on the results of an earlier survey study<sup>10</sup> concerning  $\alpha$ -particle energy spectra and angular distributions with respect to the spin direction for a number of compound nuclear systems. The two typical cases of the closed shell  $^{114}\text{Sn}^*$  and the rare earth  $^{170}\text{Yb}^*$  deexciting compound nuclei are compared. The alpha emission properties of these systems are described by the anisotropy coefficients of

the alpha particle emission with respect to the spin direction as a function of the  $\alpha$ -particle energy and  $\gamma$ -ray multiplicity. Differences in the emission patterns, in the energy region below the evaporation Coulomb barrier, suggest nearly spherical and deformed emission shapes in the cases of  $^{114}\text{Sn}^*$  and  $^{170}\text{Yb}^*$ , respectively. Assuming spherical emitters, statistical model calculations which describe closely the decay of  $^{114}\text{Sn}^*$  show discrepancies in the other system. These discrepancies, appear as (a) an underestimate of the subbarrier  $90^\circ$  CM spectra, (b) underestimates of subbarrier yields of the multiplicity-gated  $90^\circ$  CM spectra, which increase with spin, and (c) deviations in the trend of the anisotropy coefficients below the Coulomb barrier, which also increase with spin. We show that a simulation of deformation effects due to transmission accounts for these discrepancies. A detailed comparison with the  $^{170}\text{Yb}^*$  data is made, which shows the angular momentum dependence of the deformation effect in the  $\alpha$  spectra. The above findings are corroborated by both the known ground state properties and data of giant resonances built on excited states of similar compound nuclear systems.

In the second part of this paper, we report on a correlation between the shape of the proton emission spectrum and nuclear structure. Proton spectra from the  $^{52}\text{Cr}(^{24}\text{S}, 2p2n)^{32}\text{Sr}$  reaction at 130 MeV have been measured in coincidence with discrete  $\gamma$  transitions of selected exit channels. The proton spectra were observed with the Dwarf-Ball array<sup>15</sup>, a 72 CsI(Tl)  $4\pi$  detector, in coincidence with 18 Compton suppressed Ge detectors. This system was operated in conjunction with the Spin Spectrometer which recorded the associated  $\gamma$ -ray multiplicity. We found significant changes and shifts in the proton energy spectra as we selected gating transitions from different bands or transitions from states of different spin in the same band. Substantial differences were also seen as a function of the  $\gamma$ -ray multiplicity. The above results cannot be explained by statistical model calculations that do not contain explicitly nuclear structure effects. They can be explained by stretched proton emission from near-yrast states which preferentially populate the yrast band by subbarrier proton emission.

## 2. Alpha Emission Properties and Deformation Effects.

The experiments in this work were performed at the Oak Ridge Holifield Heavy-Ion Research Facility (HHIRF). The compound systems studied were  $^{110}\text{Sn}^*(E^* = 93.9 \text{ MeV})$ ,  $^{114}\text{Sn}^*(79.5 \text{ MeV})$ ,  $^{138}\text{Nd}^*$ ,  $^{164}\text{Yb}^*(67.2 \text{ MeV})$  and  $^{170}\text{Yb}^*(134.8 \text{ MeV})$ . The details of the experimental method and some of the general features of the data can be found in the current literature.<sup>8,9,10,14</sup> The complete study has been published in Ref. 16. Below, we present only the distinct features shown in the deexcitation data of  $^{114}\text{Sn}^*$  and  $^{170}\text{Yb}^*$ .

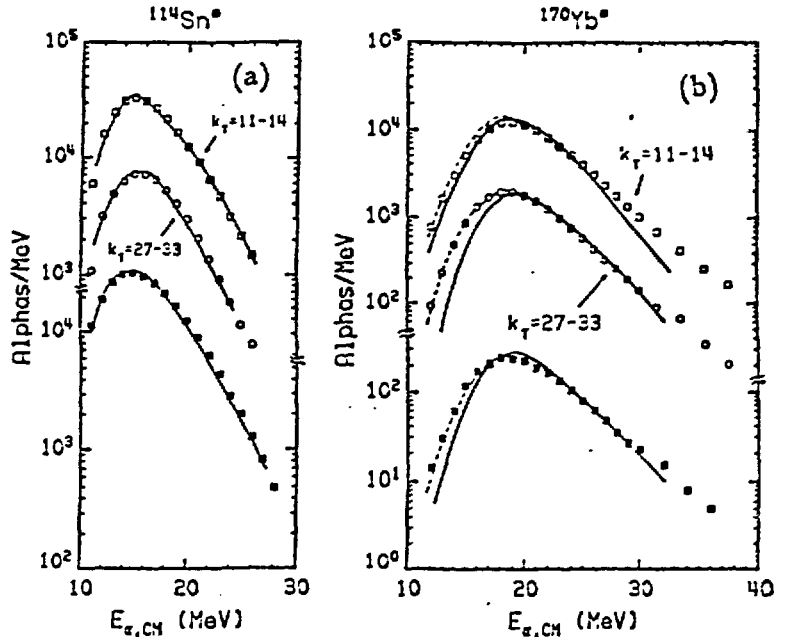
The compound nuclei  $^{114}\text{Sn}^*$  and  $^{170}\text{Yb}^*$  were produced in the reactions  $^{64}\text{Ni}(250 \text{ MeV}) + ^{50}\text{Ti} \rightarrow ^{114}\text{Sn}^*$  and  $^{20}\text{Ne}(176.6 \text{ MeV}) + ^{150}\text{Nd} \rightarrow ^{170}\text{Yb}^*$ , respectively. In this study, self-supporting targets of high isotopic enrichment in each of the isotopes were used. The  $\alpha$ -particles emitted in the deexcitation of the above compound nuclei were recorded by Si surface barrier telescopes positioned at the laboratory angles corresponding to  $\sim 90^\circ$  in the center-of-mass system.

The  $\Delta E$  detectors had thickness of  $65 \mu\text{m}$  and an acceptance cone of  $\sim 6^\circ$  half angle. The  $E$  detectors were  $1500 \mu\text{m}$  thick and served as the triggers of the spin spectrometer. The spin spectrometer served as the  $\gamma$ -ray detector and measured simultaneously the  $\gamma$ -ray multiplicity,  $M_\gamma$ , the total  $\gamma$ -ray deexcitation energy and the  $\gamma$ -ray angular correlations. In these experiments the spin spectrometer provided a coverage of 95.8% of  $4\pi \text{ sr}$ .

For each compound nuclear system ( $A_{CN}$ ,  $Z_{CN}$ ), the  $\alpha$ -particle events were transformed in the center-of-mass system for  $\alpha + (A_{CN} - 4, Z_{CN} - 2)$ , using two-body kinematics. The method used for determining the estimated spin direction is based on the emission of  $\gamma$  radiation with a particular angular relationship to the spin direction.<sup>8,14,16</sup> The  $\gamma$ -cascades from rotational nuclei formed in heavy-ion fusion-evaporation reactions have a preponderance of stretched E2 transitions which exhibit a doughnut-like pattern about the spin axis. The spin direction is identified with the short symmetry axis of this pattern. This is close to the compound nucleus spin, i.e. perpendicular to the beam, provided that the misalignment caused by particle emission is small. The  $\gamma$ -pattern for each event was projected on a plane perpendicular to the beam direction and centroid-searching methods were used to determine the angle between the short symmetry axis and the direction of the emitted  $\alpha$ -particle.

In the following analysis,  $\alpha$ -particle events corresponding to emission angles near  $\theta_{CM} = 90^\circ$  were sorted, imposing different  $\gamma$ -coincidence fold ( $k_\gamma$  gates, or angle with respect to spin ( $\beta$ ) gates. Some useful remarks can be made from an inspection of multiplicity decomposed spectra. Fig. 1(a) shows, for  $^{114}\text{Sn}^*$ , the experimental  $\theta_{CM} = 90^\circ$  spectra corresponding to  $k_\gamma = 11-14$  and  $k_\gamma = 27-33$ . The closed squares on the bottom show the total  $90^\circ$  center-of-mass spectrum integrated over  $k_\gamma$  (for  $k_\gamma \geq 11$ ) and  $\beta$ . The corresponding  $\alpha$ -particle spectra for  $^{170}\text{Yb}^*$ , under the same gating conditions, are shown in Fig. 1(b). In both cases, the selected  $k_\gamma$  bins correspond to  $\alpha$ -particle emission from nuclei with an average spin of  $\approx 34 \hbar$  and  $\approx 64 \hbar$ , respectively, deduced from statistical model calculations<sup>8,10,16</sup>.

Figure 1. (a)  $\gamma$ -fold gated  $90^\circ$  center-of-mass  $\alpha$ -particle spectra from the deexcitation of  $^{114}\text{Sn}^*$ . The open squares correspond to  $k_\gamma = 11-14$  and the open circles to  $k_\gamma = 27-33$ . The closed squares show the  $90^\circ$  center-of-mass spectrum integrated over  $k_\gamma$  and  $\beta$ . (b)  $\gamma$ -fold gated  $90^\circ$  center-of-mass alpha-particle spectra from  $^{170}\text{Yb}^*$ . The squares correspond to  $k_\gamma = 11-14$  and the circles to  $k_\gamma = 27-33$ . The closed squares show the  $90^\circ$  center-of-mass spectrum integrated over  $k_\gamma$  and  $\beta$ . The solid and dashed lines are the results of calculations described in the text.



A common trend in both cases is that the  $k_\gamma = 11-14$  spectra are slightly harder than the  $k_\gamma = 27-33$  ones. This can be understood in terms of the higher excitation energy selection made by the low  $k_\gamma$  gate. However, the subbarrier trends of the spectra are quite different. For  $^{114}\text{Sn}^*$ , the low  $k_\gamma$  compared to the high  $k_\gamma$  spectrum has an excess of subbarrier alphas, whereas these two regions in the  $^{170}\text{Yb}^*$  spectra are very similar. The solid lines in Fig. 1(a) are the result of a statistical model calculation with standard parameters.<sup>8,16</sup> We see that there is a good agreement with the data in the whole energy range, for all of the gating conditions. The corresponding calculation for  $^{170}\text{Yb}^*$  is shown, on Fig. 1(b), by the solid lines. The  $k_\gamma = 11-14$  spectrum is underpredicted in the subbarrier region as well as at high energies. In the  $k_\gamma = 27-33$  bin, the discrepancy is only in the subbarrier region and it has increased. Similarly, the total  $\alpha$  spectrum is underpredicted at subbarrier energies. In summary, although the behaviour of the  $\alpha$ -particle spectra from  $^{114}\text{Sn}^*$  is well described by statistical model calculations, we observe a systematic underprediction of the subbarrier parts of the  $^{170}\text{Yb}^*$  spectra, in a manner which increases with spin.

A striking difference is observed in the trend of the anisotropy coefficients of  $\alpha$  emission with respect to the spin direction. The anisotropy coefficients  $A_2$  (of a Legendre polynomial expansion) are plotted for the two systems as a function of  $E_{\alpha,C.M.}$  for the indicated  $k_\gamma$  bins in Fig. 2. For  $^{114}\text{Sn}^*$ , we have monotonically decreasing  $A_2$  coefficients (increasing anisotropies) with increasing  $E_\alpha$ , in each of the  $k_\gamma$  bins. In contrast with these

findings, the  $A_2$  coefficients for  $^{170}\text{Yb}^*$  have a maximum value (minimum anisotropy) at the evaporation Coulomb barrier ( $\approx 20$  MeV for  $^{170}\text{Yb}^*$  assumed spherical) and become more negative (larger anisotropies, with stronger emission perpendicular to the spin direction) at lower and higher  $E_\alpha$  values. Compared with the almost linear decrease with  $E_\alpha$  observed for  $^{114}\text{Sn}^*$ , we see a deviation in the trend of the experimental correlations below the Coulomb barrier. The  $^{170}\text{Yb}^*$  data suggest enhanced anisotropies which become larger with decreasing  $E_\alpha$ . This enhancement increases with increasing spin.

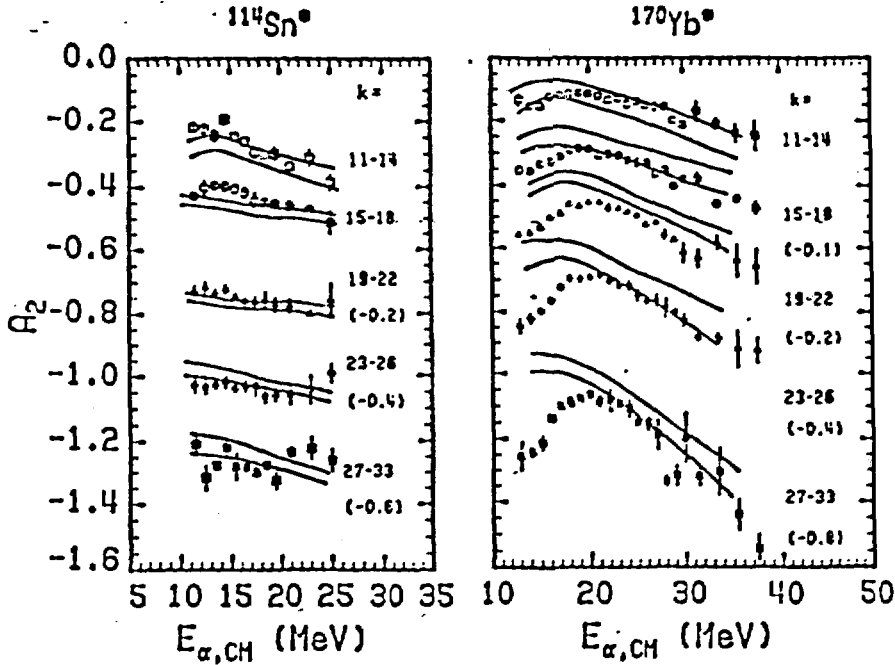


Figure 2.  $A_2$  coefficients as a function of  $E_{\alpha,C.M.}$  from the  $^{114}\text{Sn}^*$  and  $^{170}\text{Yb}^*$  systems. In both cases, the open squares, circles, closed triangles, diamonds and closed squares correspond to the  $k_7$  bins of 11-14, 15-18, 19-22, 23-26 and 27-33, corresponding to  $\langle I \rangle_\alpha$  for  $\alpha$  emission of 34, 43, 51, 59, and 64  $\hbar$ , respectively. In some cases the data have been shifted along the  $A_2$ -axis by the indicated amount. The pairs of curves are FWHM boundaries of the  $A_2$  coefficients from a statistical model calculation using transmission coefficients from a spherical optical model potential.

Both of the data sets are compared with the results of a statistical model calculation with standard parameters in Fig. 2. For  $^{114}\text{Sn}^*$ , we see that the trend of the  $A_2$  coefficients and their absolute magnitude are reproduced by the calculation.

The calculated  $A_2$  coefficients, for  $^{170}\text{Yb}^*$ , agree well with the monotonic decrease of the experimental  $A_2$  values above the Coulomb barrier, but do not reproduce the decrease of  $A_2$  at low  $E_\alpha$ .

The fact that the observed deviation occurs at emission energies sensitive to barrier penetration effects, has suggested the nuclear deformation as a possible factor for the

decrease of the measured  $A_2$  coefficients at low  $E_\alpha$ . If the emitting system is deformed with its longest axis perpendicular to the spin direction, the subbarrier  $\alpha$ -particles will be emitted preferentially along this direction (because of the lower Coulomb barrier). This leads to decreasing  $A_2$  coefficients with decreasing  $E_\alpha$ . On the other hand, the  $\alpha$ -particles above the barrier would not be affected much by the deformation since their emission is mainly determined by the level densities. Therefore, the observed deviation can be interpreted as a deformation effect which increases with spin. The same interpretation accounts also for the discrepancies observed in the multiplicity gated spectra of Fig. 1.

An interesting comparison of the above systems has been made with data from the decay of giant resonances built on excited states of similar compound nuclear systems. Giant resonance data from the decay of  $^{166}\text{Er}^*$  (61.5 MeV) suggest a two-component resonance in contrast to the decay of  $^{108}\text{Sn}^*$  (61.2 MeV) where a single resonance peak was observed.<sup>5</sup>

A simulation of deformation effects in the statistical model code was performed in the case of  $^{170}\text{Yb}^*$ , in order to get an estimate of the effect. For this purpose we employed a variation of the method of equivalent spheres<sup>18</sup>, which has been used successfully in the description of subbarrier fusion data with statically deformed targets.

The daughter nucleus was assumed to have a prolate axially symmetric shape described by the deformation parameter  $\beta$ , which was parametrized as  $R(\theta) = R_0[1 + X(\beta) + \sqrt{5/4\pi}\beta P_2(\cos\theta)]$ , where  $\theta$  is the angle with respect to the symmetry axis and  $X(\beta) = -\beta^2/4\pi$  is the volume conservation term. Optical model transmission coefficients for protons and alphas were calculated, for all of the nuclei in the cascade, at 9 different angles from  $5^\circ$  to  $85^\circ$  in steps of  $10^\circ$ . At each angle, the optical model radii were scaled according to the above equation. The diffuseness of the Woods-Saxon nuclear potential of the spheroid was also modified, so that the normal derivative at each point on an equipotential surface is unaffected by the deformation. In the evaporation calculations, charged-particle emission from a particular point of the surface of the emitting nucleus was selected with a random number weighted by the corresponding surface element of the spheroid:  $2\pi R^2(\theta)\sin\theta\Delta\theta/S$ , where  $S$  is the nuclear surface:  $S = 4\pi R_0^2(1 + a_2^2/5)$ ,  $a_2 = \sqrt{5/4\pi}\beta$ , including the first order correction term due to deformation.

The results of this calculation for the  $90^\circ$  center-of-mass spectra of  $^{170}\text{Yb}^*$  are shown in Fig. 1, by the dashed lines. A deformation of  $\beta = 0.2$  was initially assumed. The result of this calculation for the total alpha spectrum is shown on the bottom of Fig. 1(b) by the dashed line and provides a good description of the spin integrated spectrum.

On the same plot, the dashed line for the  $k_\gamma=11-14$  bin ( $\langle I \rangle_\alpha = 34\hbar$ ), shows the calculated spectrum with  $\beta=0.2$ . The subbarrier data points lie between the curves  $\beta=0$  and  $\beta=0.2$ . In this case, a deformation somewhat smaller than  $\beta=0.2$  is required to fit the

spectrum. On the other hand, for the high spin case  $k_\gamma=27-33$  ( $\langle I \rangle_\alpha=64\hbar$ ),  $\beta=0.2$  was insufficient to account for the excess of subbarrier alphas. The dashed curve in the figure, corresponds to  $\beta=0.35$  and fits closely the spectrum. These calculations demonstrate the extent and the angular momentum dependence of the effect. The originally deduced  $\beta=0.2$  was based on the total  $90^\circ$  center-of-mass spectrum and represents an average over different deformed shapes.

The calculated  $A_2$  coefficients, using the above logic, show a trend approaching the experimental data at subbarrier energies. However, no quantitative statement can be made from such comparisons, because our present formalism for the calculation of the angular correlations is limited to spherically symmetric emitters. More refined calculations are required for this purpose.

Summarizing, the distinct differences in the alpha decay properties of the compound nuclei  $^{114}\text{Sn}^*$  and  $^{170}\text{Yb}^*$  have been interpreted in terms of deformation effects. For  $^{170}\text{Yb}^*$ , our calculations have demonstrated the angular momentum dependence of the effect in the  $90^\circ$  center-of-mass spectra, besides the one observed in the trend of the anisotropy coefficients of alpha emission with respect to the spin direction. One should keep in mind that the  $\alpha$ -particle emission probe for studying nuclear shapes at high ( $E^*, I$ ) involves a broad range of initial excitation energies which contribute in low energy particle emission.<sup>16</sup>

### 3. Structure Effects and Proton Evaporation Spectra.

Compound nuclei that decay to residual nuclei with large deformations, such as superdeformed nuclei with discrete level structures, may be expected to have themselves significant deformations which persist to sufficiently high excitations of the order of at least one nucleon binding energy above the yrast line. In this case particle emission can be significantly influenced by nuclear shape effects. Furthermore, it is quite possible that structure effects can be observed on the shape of the charged particle evaporation spectra particularly near and below the emission barrier.

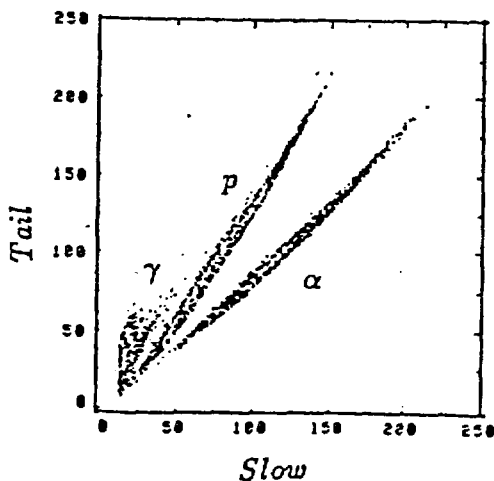
In this work we address a related issue of structural influences on the shapes of the proton spectra. We have selected for study  $^{82}\text{Sr}$  as the final nucleus, because it has been predicted to be a good candidate for superdeformation.<sup>19</sup> We have observed an unexpected strong dependence of the probability for subbarrier proton emission on the nature of the rotational bands being populated in the final nucleus.

The experiment was performed at the Oak Ridge Heavy Ion Research Facility. The  $^{82}\text{Sr}$  nuclei were produced by the  $^{52}\text{Cr}(^{34}\text{S}, 2p2n)^{82}\text{Sr}$  reaction by bombarding a stack of self-supporting  $^{52}\text{Cr}$  target foils with a 130 MeV  $^{34}\text{S}$  beam. The experimental setup consisted

of the ORNL Compton suppression spectrometer with 18 Ge detectors, which recorded the discrete  $\gamma$ -ray spectra from the reaction. The associated total  $\gamma$ -ray multiplicity and total energy were recorded with the Spin Spectrometer. The protons and  $\alpha$  particles were detected with the  $4\pi$  CsI(Tl) Dwarf Ball.<sup>15</sup> This system provided both high resolution  $\gamma$ -ray spectroscopic information and definite exit channel selection. The 72-element Dwarf Ball also provided light charged particle spectra and angular correlation information. The apparatus was triggered by two or more Ge detectors firing in coincidence with any element of the Dwarf Ball. A total of  $1.6 \times 10^8$  such events were collected and processed.

Figure 3 shows a scatter plot of the slow vs. tail map from a  $42^\circ$  CsI(Tl) detector. The  $\gamma$ -rays, protons and  $\alpha$  particles are well separated.

Figure 3. Scatter plot of the slow vs. tail light output of a CsI(Tl) detector in the Dwarf Ball showing the  $\alpha$ , proton and  $\gamma$ -ray identification. This was achieved by placing two time gates 400 ns (slow) and 1500 ns (tail) wide starting at times 0 and 1500 ns from the front of each pulse, respectively, and integrating the corresponding charge.



Excellent separation for all energies was achieved between proton and  $\alpha$  pulses from each other and from  $\gamma$ -rays or neutrons for the detectors forward of  $102^\circ$  in the laboratory ( $\sim 120^\circ$  center-of-mass). Protons with subbarrier energies and yields  $\sim 1/20$  of that at the most probable value could be clearly identified. Proton spectra sorted in this way contained  $\sim 65\%$  of the total proton yield. At larger angles due to kinematic forward focussing some of the subbarrier protons cannot be distinguished from  $\alpha$  particles and therefore the detectors at these angles were used for channel selection, but not for particle spectra. The measured overall detection efficiency for protons was 85% of  $4\pi$  (67 detectors out of 72 were used). This resulted in  $\sim 28\%$  of the events with two protons to be identified as involving only one proton. The Ge energy spectra coincident with 2 protons involved primarily  $^{82}\text{Sr}$   $\gamma$ -rays with no contamination from the  $1pxn$  or the  $\alpha xn$  emitting channels. In the most forward detectors the counting rate was  $\sim 7000$  c/s. A close examination of proton and  $\alpha$  particle spectra recorded on different tapes revealed gain shifts up to 8% in the tail component, while the slow component was considerably more stable. Gain shift corrections were applied to the tail component for every  $2 \times 10^6$  events. This ensured

good particle identification for the complete data set. The more stable slow component was energy calibrated using the  $^{12}\text{C}(p, p')$  reaction at 9.0 and 20.0 MeV. The energy calibration uncertainties were estimated to be less than 3% for all but the  $24^\circ$  detectors for which uncertainty may be as large as 6%.

The particle energies were converted event by event to the center-of-mass system. The centroid angles for each detector in the laboratory system were used in deriving the center-of-mass energy and angle, assuming two-body kinematics. Proton energy spectra were sorted using the detectors forward of  $102^\circ$ , when 2 protons were identified in the complete Dwarf Ball and for three  $k_\gamma$  gates of 3-9, 10-14, and 15-25. Further selection was made by placing gates on discrete  $\gamma$ -rays associated with various rotational bands. The background to the proton spectra associated with the underlying Compton contribution in the Ge peaks were subtracted by placing equal width gates near each  $\gamma$  peak. Care was exercised to avoid peaks that are known to be doublets. Thus, for the four main bands, gates placed on single  $\gamma$ -ray peaks for transitions up to spin 10 gave spectra of good statistical quality. For higher spins, the proton spectra for two or three transitions were added to provide spectra of improved statistical quality, but in each case the spectra for each gate were examined for consistency.

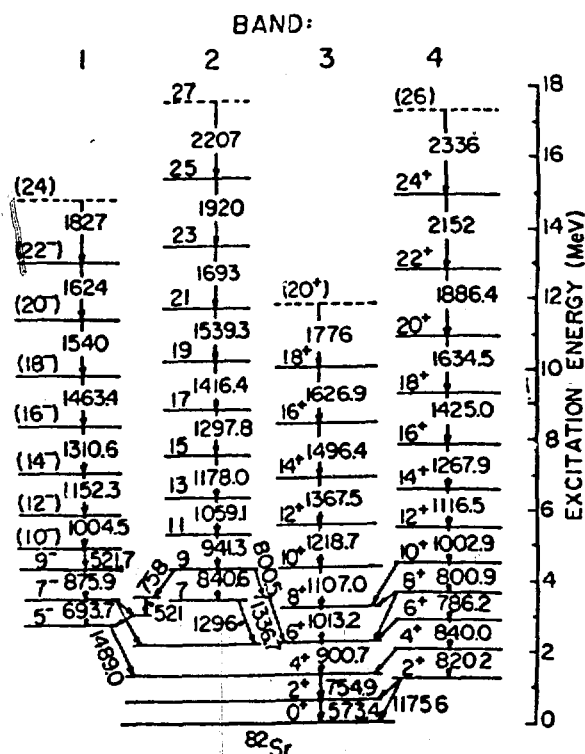


Figure 4. Partial level scheme for  $^{82}\text{Sr}$  showing four major rotational bands. Band 3 is the ground band, and band 4 is the yrast one. The odd-spin band 2 becomes yrast at spins higher than 23.

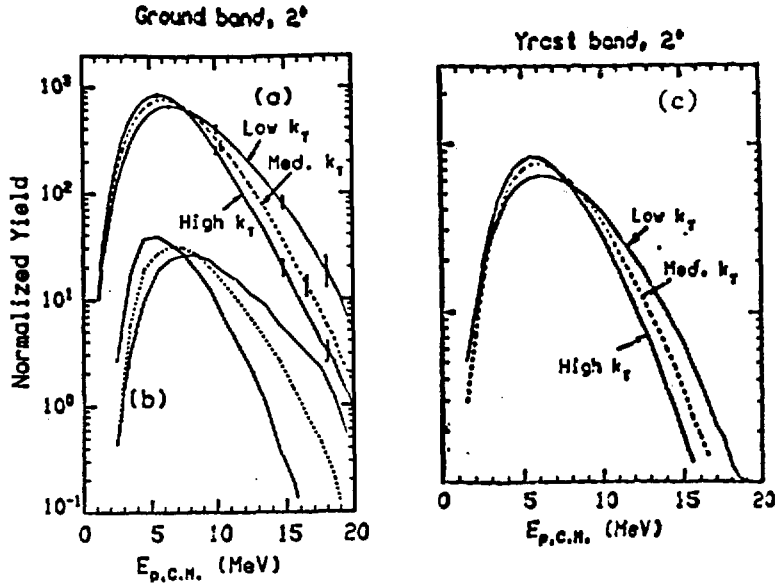


Figure 5. (a) Proton spectra coincident with the  $2^+ \rightarrow 0^+$  transition in the ground band (band 3 in Fig. 4) of  $^{82}\text{Sr}$  for the three  $k_\gamma$  gates indicated. The spectra are normalized to the same area for comparison [(peak counts)/(0.5 MeV) are  $8036 \pm 135$ ,  $25025 \pm 213$ , and  $15369 \pm 171$ , respectively. Typical statistical error bars are shown for selected bins. (b) Normalized theoretical proton spectra calculated with the evaporation code PACE for the three  $\gamma$ -ray multiplicity gates corresponding approximately to the  $k_\gamma$  bins in (a). (c) shows the center-of-mass proton spectra coincident with the  $2^+$  level in band 4 (see Fig.4) for the three  $k_\gamma$  gates. Here the proton emission barrier is essentially independent of the  $k_\gamma$  gating, although the high energy yield decreases as  $k_\gamma$  increases.

Angular correlations of the coincident protons were recorded at  $24^\circ$ ,  $42^\circ$ ,  $50^\circ$ ,  $63^\circ$ ,  $68^\circ$ , and  $78^\circ$  in the laboratory, corresponding to angles ranging from  $\sim 30^\circ$  to  $95^\circ$  in the center of mass.

The level scheme for  $^{82}\text{Sr}$  was constructed from a  $\gamma$ - $\gamma$  matrix obtained by requiring that at least one proton was detected and that the  $\gamma$ -ray multiplicity exceeded 10. The matrix thus constructed was dominated by  $\gamma$ -rays from  $^{82}\text{Sr}$ . Figure 4 shows a partial level scheme for  $^{82}\text{Sr}$  constructed from these data. Two new bands were established and four previously known bands were extended from 20 to 27  $\hbar$ . The even parity band 4 is yrast for spins between 10 and 22  $\hbar$ . The odd-spin band 2 becomes yrast for  $I \geq 23$ .

Proton spectra coincident with the  $2^+ \rightarrow 0^+$  ground transition are shown in Fig. 5(a) for the three  $k_\gamma$  gates. For purposes of comparison, the spectra are shown normalized to the same total counts. For the higher  $k_\gamma$  gates the spectra shift to lower energies and become narrower, but the high energy slopes (above  $\sim 15$  MeV) for all  $k_\gamma$  gates are similar. This is understood in terms of the decreasing available thermal energy as  $k_\gamma$  or equivalently the spins of the entry region are increased (the three  $k_\gamma$  gates correspond to  $I \sim 4$ -19, 17-29, and 26-45  $\hbar$ , and to average yrast energies of  $\sim 7$ , 14 and 23 MeV, respectively). A

statistical-model calculation with the evaporation code PACE<sup>17</sup> for this system reproduces these features at least qualitatively. This is shown in Fig. 5(b). In contrast to this, the proton spectra associated with the  $2^+$  level of band 4 (non-yrast at this spin, but yrast at spins 12 to  $22\hbar$ ) show similar peak positions for the three  $k_\gamma$  gates (Fig. 5c). Again, as the  $k_\gamma$  is increased, the spectra also become narrower but at higher energies the slopes are similar. These differences between the spectra coincident with two different  $2^+$  states suggest that some structural effects and/or feeding patterns may be responsible.

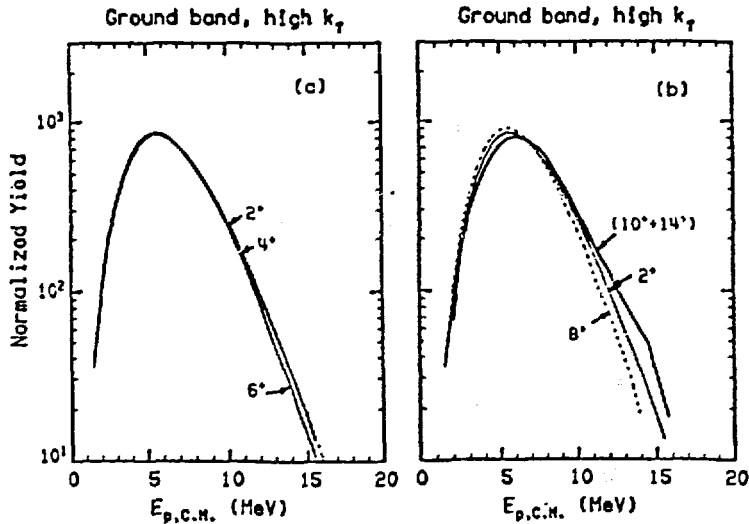


Figure 6. Panel (a) shows proton spectra coincident with  $\gamma$ -rays from the  $2^+$ ,  $4^+$ , and  $6^+$  levels in the ground band 3 for the high  $k_\gamma$  gate. The spectra are normalized to the same total counts for ease of comparison. The spectra are remarkably similar. Panel (b) shows proton spectra coincident with the  $8^+$  and the sum of ( $10^+ + 14^+$ ) levels in the same ground band 3 and for the high  $k_\gamma$  gate. The  $2^+$  spectrum is also shown for comparison. Significant differences are seen (see text).

In order to explore any dependence of the proton emission probability on the structure of the final nucleus, we have compared in Fig. 6(a) the proton spectra coincident with the  $\gamma$ -rays from the  $2^+$ ,  $4^+$ , and  $6^+$  states in the ground band 3 and for the high  $k_\gamma$  gate. Clearly, the spectra are very similar. This is understood from the fact that the  $2^+$ , the  $4^+$  and for the most part the  $6^+$  levels receive practically all their feeding from all the bands in  $^{82}\text{Sr}$ .

In contrast, the  $8^+$  level in the same band 3 is fed from higher spin members of the ground band and to a significant fraction by the yrast band 4. Levels above the  $8^+$ , however, are only populated by the decay of the levels of the continuation of the ground band. The proton spectra coincident with the  $8^+$  and the sum of  $10^+$  and  $14^+$  levels are compared in Fig. 6(b) with the  $2^+$  spectrum. It is seen that the spectra for the  $8^+$  and

( $10^+ + 14^+$ ) levels have most probable values that shift toward lower and higher energies, respectively. These unexpected shifts are consistent with the behavior of the spectra associated with the high spin states in the four major bands in  $^{82}\text{Sr}$ .

If we further examine the proton spectra from individual levels within each band having spins higher than  $10\hbar$  we find them to be similar to each other, but they differ considerably if they are associated with different bands. Thus, the proton spectra associated with transitions from the levels with spin 11, 13, and (19+23) in the odd spin band 2 of  $^{82}\text{Sr}$  were found to be essentially identical in shape.

In contrast, when we compare proton spectra associated with high spin levels ( $\geq 10\hbar$ ) at comparable excitation energies from different bands, large differences are found for all three  $k_\gamma$  gates. This is clearly seen in Fig. 7, where proton spectra associated with the sum of the  $10^+$  and  $14^+$  levels in the ground band 3 (dashed line), the  $I=13$  level of band 2 (thin line), and the sum of the  $14^+$  and  $16^+$  levels of the yrast band 4 (thick line) are shown for the high  $k_\gamma$  gate. The striking feature in these spectra is that for the same  $k_\gamma$  gate, the peak in the proton spectrum shifts down by 1 MeV in going from band 3 to band 2 and then to the yrast band 4. This is comparable in magnitude to the shifts seen in Fig. 5(a) for the  $2^+ \rightarrow 0^+$  transition from the low to the high  $k_\gamma$  gate.

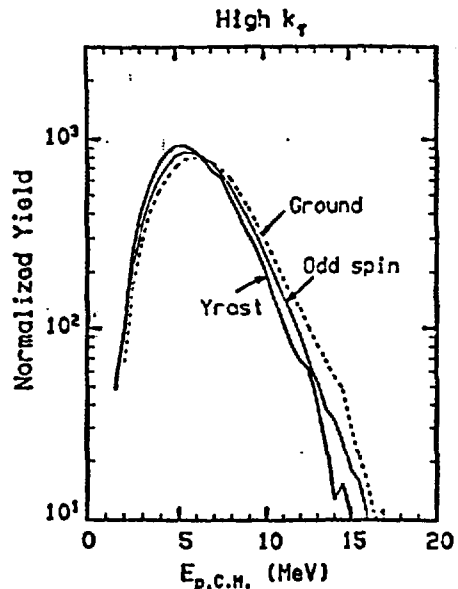
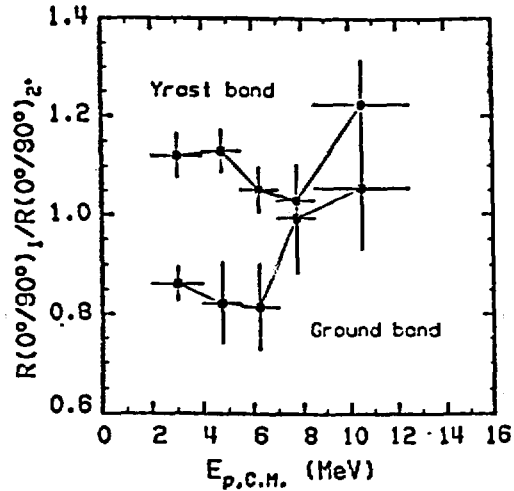


Figure 7. Proton spectra from the high  $k_\gamma$  gate coincident with transitions from the ( $10^+ + 14^+$ ) levels of the ground band 3 (dashed line), from the  $I=13$  level of the odd spin band 2 (thin line), and from the ( $14^+ + 16^+$ ) levels in the yrast band 4 (thick line). Shifts as large as 1 MeV are seen in going from the ground to the yrast band gates.

These results are surprising since the entry states are expected to lie at considerably higher excitation energies than the gating transitions and any correlation between the proton spectrum and the nature of the band being populated ought to be washed out by the statistical gamma emission. In fact, somewhat higher thermal energy is available for the yrast band 4 and this should shift its associated proton spectrum in the opposite direction. A possible explanation might be that although we have the same  $k_\gamma$  gate, the

yrast band is populated from entry regions of higher spins compared to the ground or the other bands. This could cause a shift analogous to that in Fig. 5(a).

Figure 8. Anisotropy ratios for the protons from high  $k_\gamma$  gate coincident with the high spin transitions (Fig. 7) in the yrast band 4 (full squares) and the ground band 3 (open squares), relative to that for the  $2^+ \rightarrow 0^+$  transition to the ground state. The horizontal error bar give the widths of the proton energy gates used. These were chosen to give comparable statistics in the correlations. Note that a ratio smaller than unity means that the anisotropy is smaller than that for the ground  $2^+ \rightarrow 0^+$  transition.



We can offer a strong argument against the latter simple explanation in terms of phase-space effects. We note that the energy shifts are comparable to those for the  $2^+ \rightarrow 0^+$  transition in Fig. 5(a), where the spins and excitation energies for the three  $k_\gamma$  gates are greatly different. Consequently, a comparably large difference in the entry regions of the gating transitions should be easily observed experimentally by projecting the actual  $k_\gamma$  distributions coincident with the same discrete high spin transitions. We found that the  $k_\gamma$  distributions associated with the high spin discrete  $\gamma$  gates in the four bands are identical (the average  $k_\gamma$  values for the ground, odd spin, and yrast bands were found to be  $15.5 \pm 0.2$ ,  $15.5 \pm 0.2$  and  $15.4 \pm 0.2$ , respectively). In addition, a statistical model calculation in which the high multiplicity gate was moved up by one unit produced a considerably smaller shift in the proton spectrum than observed in Fig. 7.

Another unlikely possibility would be that through fractionation the ground band samples the high total  $\gamma$  energy part of the entry region and the yrast band the lower one. This would give the yrast and ground bands less and more thermal energy, respectively. According to a statistical model calculation this does not affect the peak and subbarrier portions of the proton spectra, but shifts the high energy part in the opposite direction than observed.

A reasonable explanation for the observed large shifts in the proton spectra is suggested by the steep experimental yrast line and consequently the entry line in  $^{82}\text{Sr}$  and the energy balance in this reaction which places the entry line only a few MeV above the yrast line. This is also confirmed by statistical model calculations. These observations and the data suggest that a significant fraction of the population of the rotational bands in  $^{82}\text{Sr}$ , and

in particular the yrast band, occurs by direct proton emission from near-yrast to near-yrast states with the second proton playing that role. This mechanism could explain many features of the data and would in addition require that the last proton emission be stretched in character, particularly at and below the emission barrier, where it should exhibit a strong anisotropy  $R(0^\circ/90^\circ) \equiv W(0^\circ)/W(90^\circ)$  with respect to the beam direction. This is indeed what we observe in Fig. 8 where the anisotropy ratios for the high spin gates of Fig 7 of the ground and the yrast bands are plotted relative to the anisotropy of the  $2^+ \rightarrow 0^+$  ground transition as a function of the proton center-of-mass energy for the high  $k_\gamma$  gate. This further supports this explanation, since the direct population of the ground band has a higher Coulomb barrier compared to that for the population of the yrast band.

Proton emission from the near-yrast states may be associated with a predicted mechanism based on instability toward nucleon emission at large spins, connected with the population of  $h_{11/2}$  resonance states in nuclei in this region.<sup>20</sup> These predicted yrast proton transitions were expected to have enhanced anisotropies as observed in our work.

In summary, we have observed a strong dependence of the proton energy spectra on the nature of the final high spin states belonging to different rotational bands in  $^{82}\text{Sr}$ , which cannot be accounted for in terms of simple statistical model calculations that do not include explicitly nuclear structure effects. The large shifts toward lower energies and the stronger anisotropies when subbarrier protons lead to high spin states in the yrast band compared to the ground band are interpreted as due to near-yrast emission of subbarrier high- $\ell$  protons that preferentially populate the yrast band. These results suggest that spectra and angular distributions of subbarrier protons may provide a sensitive probe of the structure of excited, highly spinning nuclei.

The authors acknowledge fruitful discussions with T. Døssing. The assistance of X.T. Liu during the data acquisition for the last experiment is appreciated. M.A.R. and A.V. acknowledge support from the Joint Institute for Heavy Ion Research. This work was supported in part by the U.S. Department of Energy under grant No. DE-FG02-88ER-40406. Oak Ridge National Laboratory is operated by Martin Marietta Energy Systems Inc. under Contract No. DE-AC05-84OR21400 with the U.S. Department of Energy.

## References

1. P.J. Twin, B.M. Nyako, A.H. Nelson, J. Simpson, M.A. Bentley, H.W. Cranmer-Gordon, P.D. Forsyth, D. Howe, A.R. Mokhtar, J.D. Morrison, J.F. Sharpey-Schafer and G. Sletten, *Phys. Rev. Lett.* **57** (1986) 811; P.J. Nolan and P.J. Twin, *Ann. Rev. Nucl. Part. Sci.* **38**, 533 (1988) and references therein.

2. J. Dudek, T. Werner and L.L. Riedinger, *Phys. Lett.* B211, 252 (1988).
3. S. Cohen, F. Plasil, and W. Swiatecki, *Ann. of Physics, N.Y.* 82, 557 (1974).
4. L.A. Goodman, *Phys. Rev.* C37, 2162 (1988).
5. K.A. Snover, *Ann. Rev. Nucl. Part. Sci.* 36, 545 (1986).
6. M.Blann and T.T.Komoto, *Phys. Scr.* 24, 93 (1981).
7. J.M. Alexander, D.Guerreau and L.C. Vaz, *Z. Phys.* A305, 313 (1982).
8. F.A. Dilmanian, D.G. Sarantites, M. Jääskeläinen, H. Puchta, R. Woodward, J.R. Beene, D.C. Hensley, M.L. Halbert, R. Novotny, L. Adler, R.K. Choudhury, M.N. Namboodiri, R.P. Schmitt, and J.B. Natowitz, *Phys. Rev. Lett.* 49, 1909 (1982).
9. Z. Majka, D.G. Sarantites, L.G. Sobotka, K.J. Honkanen, E.L. Dines, L.A. Adler, Ze Li, M.L. Halbert, J.R. Beene, D.C. Hensley, R.P. Schmitt and G. Nebbia, *Phys. Rev. Lett.* 59, 322 (1987).
10. N.G. Nicolis, D.G. Sarantites, L.A. Adler, F.A. Dilmanian, K.J. Honkanen, Z. Majka, L.G. Sobotka, Z. Li, T.M. Semkow, J.R. Beene, M.L. Halbert, D.C. Hensley, J.B. Natowitz, R.P. Schmitt, D. Fabris, G. Nebbia and G. Mouchaty, 'The Variety of Nuclear Shapes', edited by J.D. Garrett, C.A. Kalfas, G. Anagnostatos, R. Vlastou, (World Scientific, 1987) pp. 526-536.
11. Z. Majka, M.E. Brandan, D. Fabris, K. Hagel, A. Menchaca-Rocha, J.B. Natowitz, G. Nebbia, G. Prete, B. Sterling and G. Viesti, *Phys. Rev.* C35, 2125 (1987).
12. L.C. Vaz and J.M. Alexander, *Z. Phys.* A318, 231 (1984).
13. M. Jääskeläinen, D.G. Sarantites, R. Woodward, F. A. Dilmanian, J.T. Hood, R. Jääskeläinen, D.C. Hensley, M.L. Halbert, and J.H. Barker, *Nucl. Instr. Meth.* 204, 385 (1983).
14. K.J. Honkanen, F.A. Dilmanian, D.G. Sarantites, and S.P. Sorensen, *Nucl. Instr. Meth.* 257, 233 (1987).
15. D.W. Stracener, et al., *Nucl. Instr. Meth.* (in press). A CsI(Tl) version of the Dwarf Ball system described in: D.G. Sarantites, et al. *Nucl. Instr. Meth.* A264, 319 (1987).
16. N.G. Nicolis, D.G. Sarantites, L.A. Adler, F.A. Dilmanian, K. Honkanen, Z. Majka, L.G. Sobotka, Z. Li, T.M. Semkow, J.R. Beene, M.L. Halbert, D.C. Hensley, J.B. Natowitz, R.P. Schmitt, D. Fabris, G. Nebbia, and G. Mouchaty, *Phys. Rev.* C41, 2118 (1990)
17. A. Gavron, *Phys. Rev.* C21, 230 (1980); modification PACE2S by J.R. Beene.
18. R.G. Stokstad and E.E. Gross, *Phys. Rev.* C23, 281 (1981).
19. W. Nazarewicz et al., *Nucl. Phys.* A345, 397 (1985), and private communication.
20. T. Dossing, S. Frauendorf, and H. Schulz, *Nucl. Phys.* A287, 137 (1977).